Supplemental Material

Journal of Climate

El Niño–Related Summer Precipitation Anomalies in Southeast Asia Modulated by the Atlantic Multidecadal Oscillation

https://doi.org/10.1175/JCLI-D-19-0049.1

Supplemental Material

Captions:

Figure S1 El Niño-related precipitation anomalies (unit: mm day^{-1}) in (a and c) MJ and (b and d) JA, derived from the GPCC dataset during positive phases of the AMO (the left column) and negative phases of the AMO (the right column) from 1901 to 2013. The hatched shading indicates statistical significance at the 95% confidence level according to the Student's *t*-test.

Figure S2 As in Figure S1, but for results derived from the CN05.1 dataset for the period of 1961–2014.

Figure S3 El Niño-related anomalous wave activity flux (vectors; units: m^2 s^{-2}) and geopotential height (contours; units: gpm) at 300 hPa in MJ during (a) positive phases of the AMO and (b) negative phases of the AMO for the period of 1901–2014. The shading show statistical significance at the 95% confidence level according to the Student's *t*-test.

Figure S4 El Niño-related anomalous velocity potential (shading; units: 10^6 m^2 s^{-1}) and divergent wind (vectors; units: m s^{-1}) in JA at (a) 200 hPa, and (b) 850 hPa during positive phases of the AMO for the period of 1901–2014.

Figure S5 El Niño-related anomalous (a and c) wave activity flux (vectors; units: m^2 s^{-2}) and geopotential height (contours; units: gpm) at 300 hPa, and (b and d) sea level pressure (units: Pa) derived from GFDL-CM3 in JA during (a and b) positive phases of the AMO and (c and d) negative phases of the AMO for the period of 1901–2005. The shading in (a and c), and dotted shading in (b and d) show statistical significance at the

95% confidence level according to the Student's *t*-test.

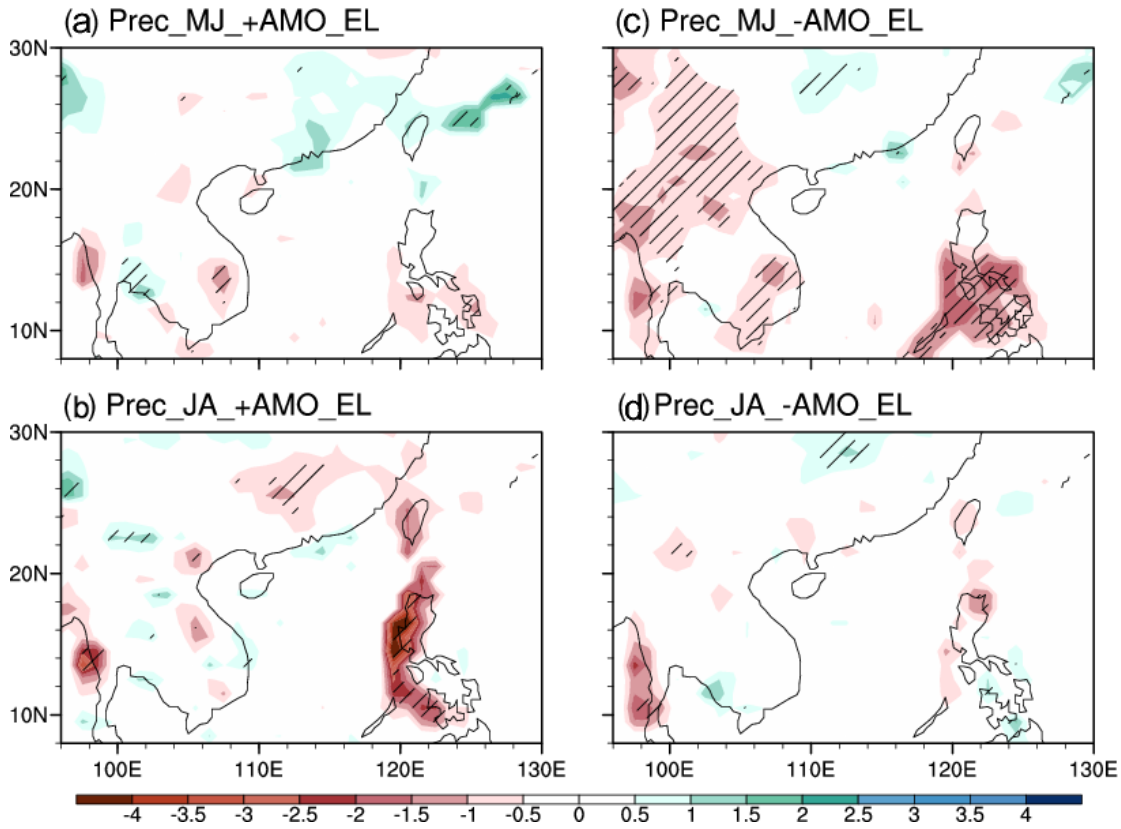

Figure S1 El Niño-related precipitation anomalies (unit: mm day^{-1}) in (a and c) MJ and (b and d) JA, derived from the GPCC dataset during positive phases of the AMO (the left column) and negative phases of the AMO (the right column) from 1901 to 2013. The hatched shading indicates statistical significance at the 95% confidence level according to the Student's *t*-test.

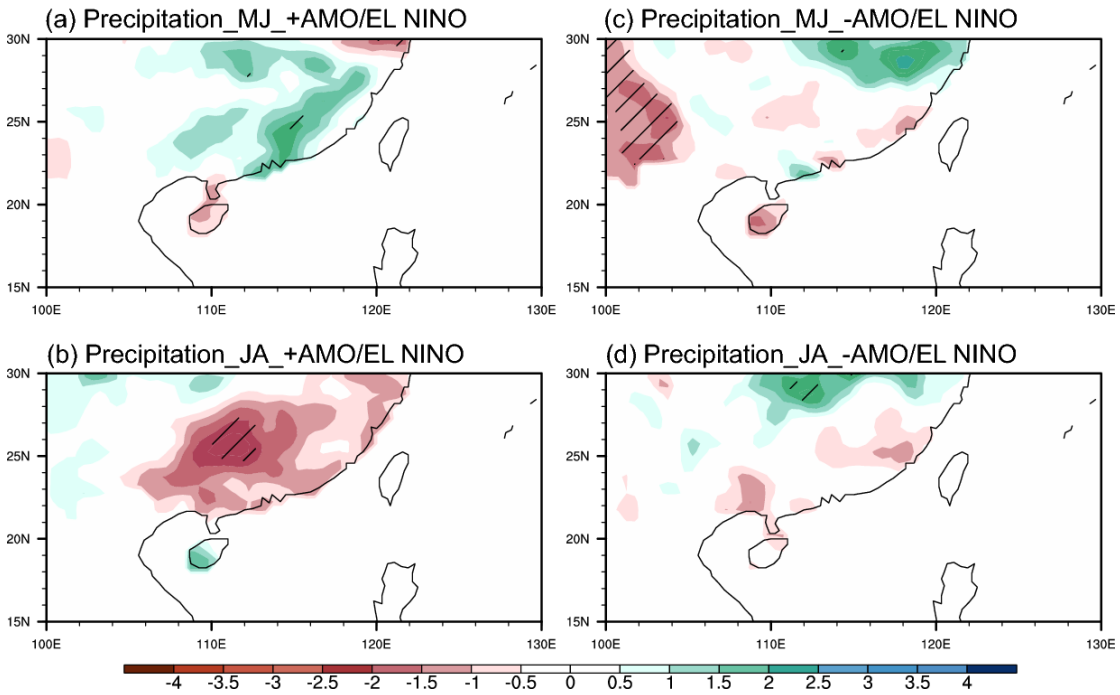

Figure S2 As in Figure S1, but for results derived from the CN05.1 dataset for the period of 1961–2014.

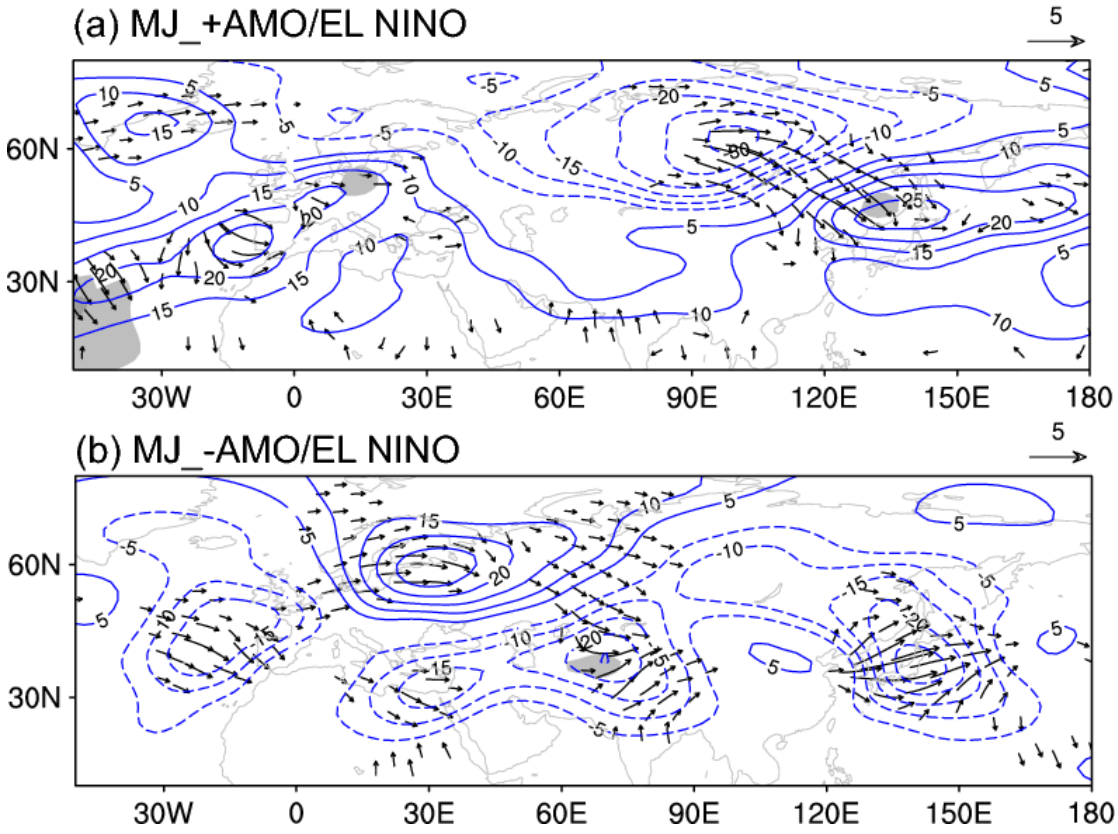

Figure S3 El Niño-related anomalous wave activity flux (vectors; units: m^2 s^{-2}) and geopotential height (contours; units: gpm) at 300 hPa in MJ during (a) positive phases of the AMO and (b) negative phases of the AMO for the period of 1901–2014. The shading show statistical significance at the 95% confidence level according to the Student's *t*-test.

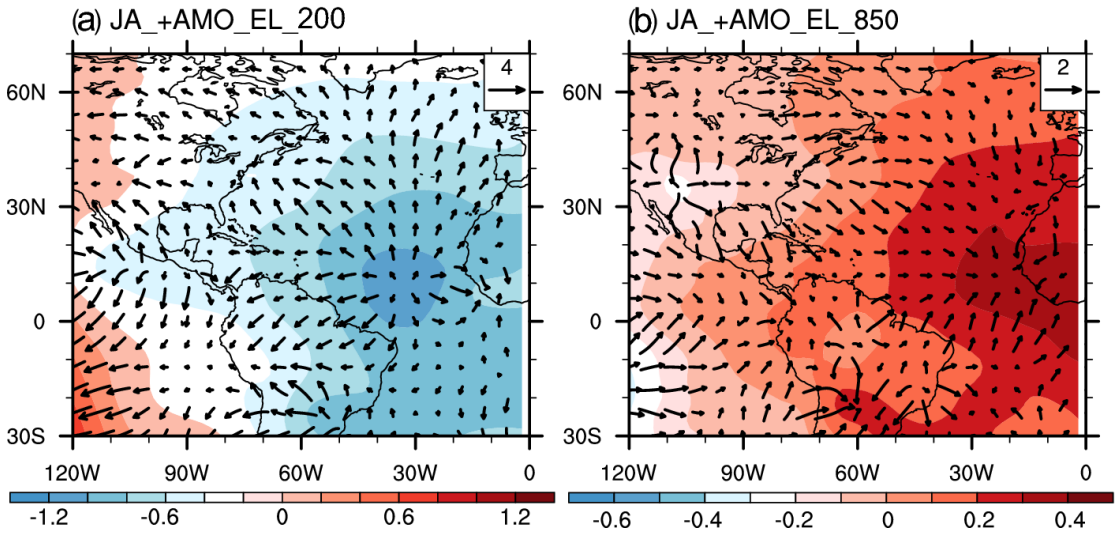

Figure S4 El Niño-related anomalous velocity potential (shading; units: 10^6 m^2 s^{-1}) and divergent wind (vectors; units: m s^{-1}) in JA at (a) 200 hPa, and (b) 850 hPa during positive phases of the AMO for the period of 1901–2014.

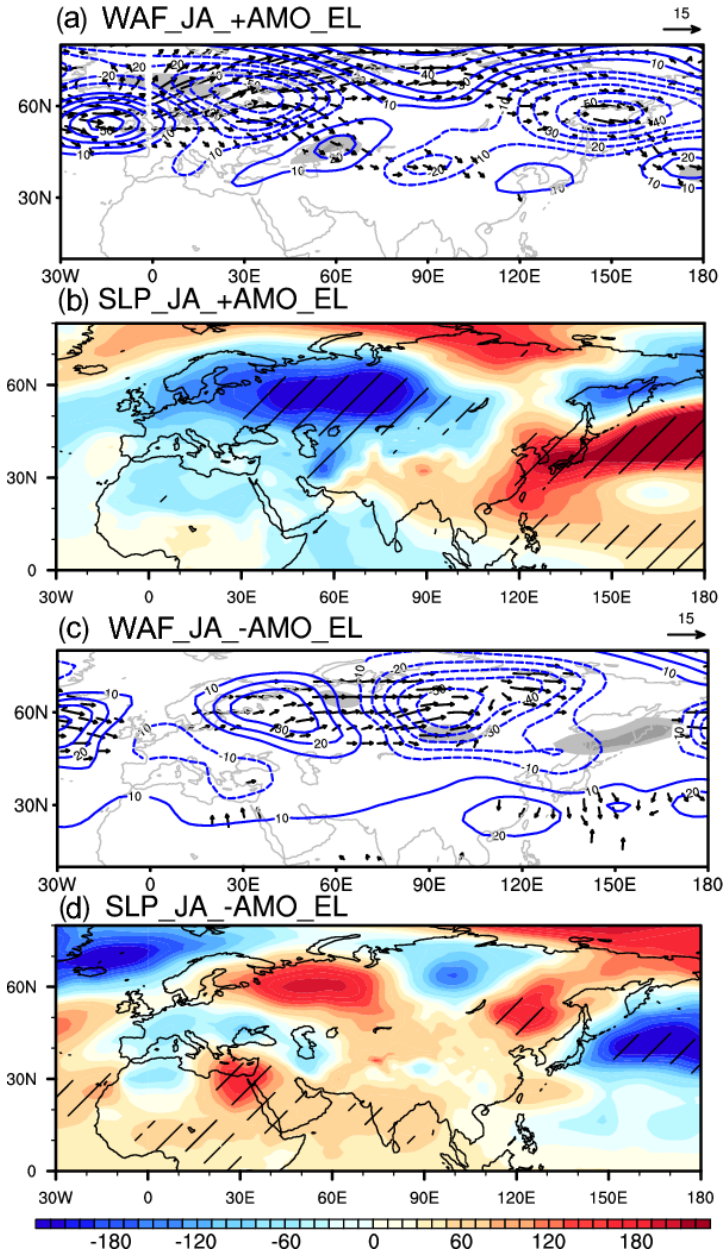

Figure S5 El Niño-related anomalous (a and c) wave activity flux (vectors; units: m^2 s^{-2}) and geopotential height (contours; units: gpm) at 300 hPa, and (b and d) sea level pressure (units: Pa) derived from GFDL-CM3 in JA during (a and b) positive phases of the AMO and (c and d) negative phases of the AMO for the period of 1901–2005. The shading in (a and c), and dotted shading in (b and d) show statistical significance at the 95% confidence level according to the Student's *t*-test.